RoSense: Refining LOS Signal Phase for Robust RFID Sensing via Spinning Antenna

Yinan Zhu, *Student Member, IEEE*, Chunhui Duan, *Member, IEEE*, Xuan Ding, *Member, IEEE*, and Zheng Yang, *Fellow, IEEE*

***Abstract*—RFID sensing leveraging backscatter signal features (e.g., phase shift) from tags has gained increasing popularity in numerous applications but also suffers from negative impacts of environmental multipaths. Past works to address it rely on extra customized devices, labor-intensive offline training, or frequency channel hopping, all of which are non-ubiquitous or ineffective for real-life adoption. This article presents *RoSense*, a universal method to alleviate multipath reflections' impacts by spinning the reader antenna, thus enabling more robust RFID sensing. Besides, RoSense requires no RF devices or offline training and operates in a nonintrusive manner. The key insight of RoSense is to exploit two properties of line-of-sight (LOS) signal when spinning the antenna, i.e., the *linearity of phase changes* and *stability of received signal strength* to attenuate the nonlinear and nonmonotonic effect of multipath signals and refine the phase shift of LOS signal. We have implemented a prototype of RoSense with COTS devices and studied two cases for evaluation: 1) material identification and 2) object localization. Experimental results show that RoSense can improve the material identification accuracy by up to 16.22% and reduce the mean localization error by up to 39.93%, greatly outperforming the state-of-the-art solutions.**

***Index Terms*—Antenna polarization, line-of-sight (LOS) signal phase refinement, multipath reflections, RFID sensing.**

I. Introduction

BEYOND identification function, RFID technology has shown its potential as battery-free, low-cost, and small-sized sensors to enable ubiquitous sensing applications, such as object localization and tracking [1], [2], material classification [3], items ordering [4], [5], spinning and vibration inspection [6], [7], and temperature and moisture measurement [8], [9]. The underlining rationale of these systems is generally leveraging the changes of backscatter signal features, typically received signal strength (RSS) and *phase shift* affected by targeted objects or events to retrodict them. Due to the low resolution of coarse-grained RSS measurement, the phase shift is much more frequently harnessed for sensing [10]. However, the multipath effect mainly induced by environmental reflections from obstacles has always been a critical problem that limits the robustness of existing RFID sensing systems [10]–[12]. The phase readings of line-of-sight (LOS) signal are easily affected by these reflected multipath signals (see Fig. 1), yielding low accuracies and large errors of sensing results.

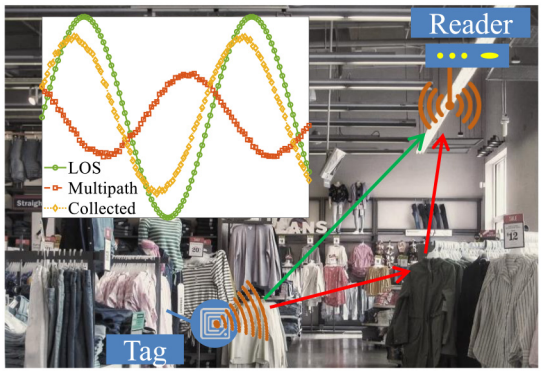

Fig. 1. Multipath effect on LOS backscatter signal.

Most works to address this problem require either extra customized RF devices (e.g., software-defined radios) for physical-layer signal processing [13], [14], which is incompatible with existing RFID infrastructure and incurs high deployment, operation, and maintenance overhead, or offline training to learn multipath profiles [15], [16], which is time consuming with a significant amount of human effort and always not cross-domain with little transferability to a new environment. The state-of-the-art work CPIX [17] is the only universal approach that exploits frequency channel hopping to cleanse the signal phase. Nevertheless, CPIX still has a lot of limitations, e.g., limited and unstable accuracy improvement, high time delay, and also incapability when the tag's impedance changes irregularly. To the best of our knowledge, such a ubiquitous solution that could effectively defend against multipaths still does not exist.

In this article, we present a more universal and effective method, namely *RoSense* that refines the LOS signal phase via spinning the reader antenna. Moreover, RoSense requires no extra RF devices, offline training, or modifications to EPC Gen2 standard [18] and operates in a nonintrusive manner. The basic idea is that the phase readings of the LOS signal

Manuscript received 10 March 2022; revised 26 May 2022; accepted 1 July 2022. Date of publication 25 July 2022; date of current version 21 November 2022. This work was supported in part by the National Key Research and Development Program of China under Grant 2018YFB0803403; in part by the National Natural Science Foundation of China under Grant 61902212; and in part by the Beijing Institute of Technology Research Fund Program for Young Scholars. *(Yinan Zhu and Chunhui Duan are co-first authors.) (Corresponding author: Chunhui Duan.)*

Yinan Zhu, Xuan Ding, and Zheng Yang are with the School of Software and BNRist, Tsinghua University, Beijing 100084, China (e-mail: zhuyn1997@gmail.com; dingx04@gmail.com; hmilyyz@gmail.com).

Chunhui Duan is with the School of Computer Science and Technology, Beijing Institute of Technology, Beijing 100081, China (e-mail: duanch@bit.edu.cn).

Digital Object Identifier 10.1109/JIOT.2022.3191947

shall linearly change with the spinning angles ideally in a multipath-free environment, but slightly deviate from linear trends in a multipath-prevalent environment because the effect of multipath signals changes nonlinearly and nonmonotonically. Similarly, RSS readings shall remain unchanged ideally when spinning, but fluctuate within a small range due to multipaths. Accordingly, we can exploit the *linearity of phase changes* and *stability of RSS* to jointly refine the LOS signal phase via optimization algorithms. First, we conduct weighted linear regression on the collected phase vector after spinning. Then, we exploit the corresponding RSS vector to calibrate the possible intercept drift in linear regression. After calibration, the refined phase is obtained. Further for real-time spinning, we address the practical problem of nonuniform sampling and prove an upper bound of performance loss as compared to fixed-interval spinning. In this way, many existing sensing systems can harvest benefits, if only RoSense acts as middleware and the refined phase readings after processing are inputted to these systems. To evaluate RoSense, we study two applications: 1) nonintrusive material identification and 2) anchor-free object localization. Experimental results demonstrate that RoSense can achieve around 16.22% improvement of material identification accuracy and 17.52%–39.93% reduction of localization error, which significantly outperforms CPIX. Note that RoSense only needs a commercial off-the-shelf (COTS) mechanical spin axis that is common to find, nonintrusive and low-cost as compared to customized RF devices like USRPs, and thus our method is more universal and practical.

Contributions: In summary, our contributions are threefold as follows.

1) We propose a more ubiquitous and effective method, namely RoSense to refine the LOS signal phase under multipaths and enable robust RFID sensing, without requiring any extra RF devices or offline training.
2) To the best of our knowledge, RoSense is the first to push forward two properties of LOS signal under antenna spinning and analyze the effects of multipath signals, based on the generalized phase model we propose. Besides, RoSense is universal for almost all types of passive tags.
3) We implement a prototype of RoSense and study two cases for evaluation. Experimental results demonstrate that our method can remarkably decrease the error of object localization and increase the accuracy of material identification, significantly outperforming the state-of-the-art solutions.

The remainder of this article is organized as follows. Section II introduces the background of RFID sensing and multipath effect. Section III elaborates our methodology mechanism and the details of system design. Section IV prototypes RoSense and Section V comprehensively evaluates it through extensive experiments. Section VI overviews the related works and their limitations. We conclude our work in Section VII.

II. Preliminary

A COTS RFID reader can generally collect around 60–87 samples per second, determined by the backscatter link frequency (BLF) and reader modes. For each sample, the reader can provide a series of tag's backscatter signal features, including RSS, phase shift, and Doppler frequency shift (DFS), along with the corresponding timestamps. We retrospect how these signal features are related to the sensing targets as follows.

RSS: The reported RSS (denoted as P) has a low resolution of only 0.5 dBm and can be expressed as

$$P = 10 \lg \frac{P_0 G_r^2 G_t^2 L \lambda^4}{(4\pi d)^4} \tag{1}$$

where d refers to the antenna–tag distance and λ is the wavelength of the RFID signal. G_r and G_t denote the antenna gain of reader and tag, respectively. P_0 denotes the transmission power of the reader antenna and L is a constant representing the transmission loss. Although RSS is related to many factors like antenna–tag distance and can be used for localization theoretically speaking [19], L is easily affected by the environment. A low measurement resolution leads to a large error. Hence, RSS is not suitable for fine-grained RFID sensing.

Phase: The reported phase shift (denoted as ϕ) has a relatively high resolution of $(2\pi/4096) \approx 0.00153$ rad and can be described by the following expression:

$$\phi = \left(\frac{4\pi}{\lambda} d + \phi_o + \phi_R + \phi_T \right) \bmod 2\pi \tag{2}$$

where ϕ_R and ϕ_T denote the phase shifts induced by the reader and tag's hardware, respectively. ϕ_o denotes the phase shift introduced by the relative orientation of the reader antenna and tag (detailedly explained in Section III-A). Hence, phase shift owns the capability of not only fine-grained localization [1], orientation detection [20] but also hardware-related sensing like material identification [3]. So, the phase shift is more frequently harnessed for sensing as compared to RSS.

DFS: The reported DFS (denoted as F_m) is actually determined by the phase rotation $\Delta\phi$ across a packet [21]. The relationship is as follows:

$$\Delta\phi = |F_m \cdot 4\pi \Delta T| \tag{3}$$

where ΔT denotes the packet duration which is related to BLF. Few works utilize DFS because it is not directly related to the sensed target, whereas $\Delta\phi$ indeed reflects the multipath conditions and can render a confidence estimation of ϕ. So this article innovatively leverages DFS in Section III-D.

Consistency: In multipath conditions, the variances of RSS, phase shift, and DFS should consist of each other. That is, if one feature fluctuates violently, the other features would not be stable likewise. To verify this, we fix a reader antenna and a tag at certain locations and collect the tag's signal features, in the clean and multipath environment, respectively. Fig. 2 depicts the measurement results. We can get two observations. First, the consistency holds and the variances under multipath (e.g., 5.884 rad of phase and 27.5 dBm of RSS) are much larger than those in the clean environment (e.g., 0.055 rad of phase and 0.5 dBm of RSS). The impact of multipath is severe and nonnegligible. Second, the amount of DFS can indeed help distinguish multipath environment, e.g., DFS under multipath reaches 250.625 Hz whereas that in the clean environment is less than 15.438 Hz. This consistency serves for Section III-C.

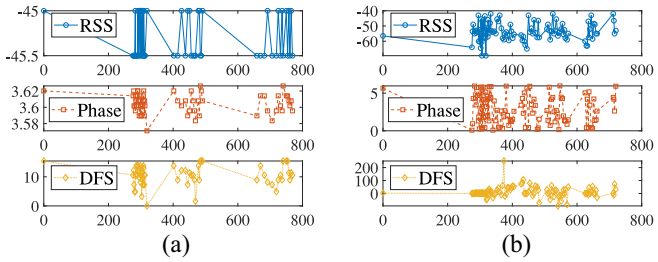

Fig. 2. Consistency of signal features. (a) Clean environment. (b) Multipath environment.

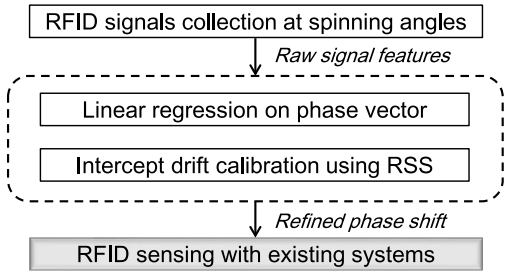

Fig. 3. System overview of RoSense.

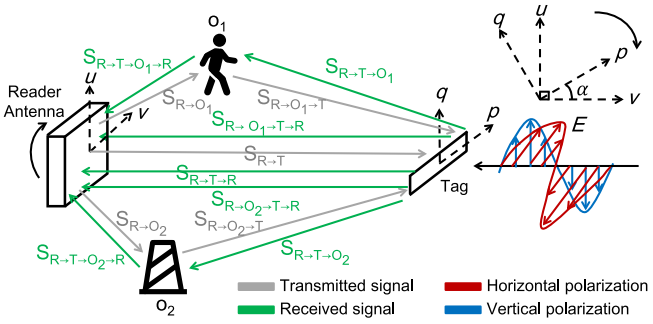

Fig. 4. Propagation of RFID signals.

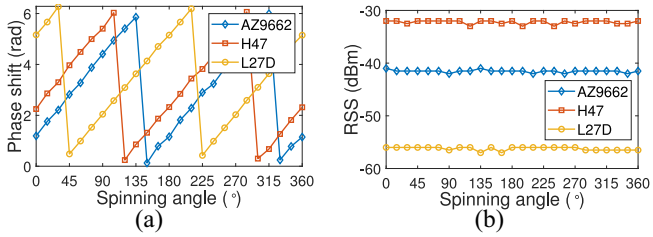

Fig. 5. Experimental verification of LOS signal's properties. (a) Linearity of phase changes. (b) Stability of RSS.

III. System Design

Fig. 3 depicts the system overview of RoSense. By spinning the reader antenna, we can obtain the vectors of signal features for LOS signal phase refinement. The workflow of RoSense contains two steps: 1) phase vector regression and 2) intercept drift calibration. We introduce the technical details as follows.

A. Mechanism of RoSense

As is well known, different antenna types of tags have distinct polarization modes, e.g., Alien AZ-9662 tags are linearly polarized, ImpinJ H47 tags are dual-linearly polarized, and ImpinJ L27D tags are circularly polarized [22], [23]. Even so, we can abstract a dual-linearly polarized or circularly polarized antenna to two orthogonal linearly polarized antennas [24].

Fig. 4 shows the practical propagation of RFID signals and we first analyze the LOS backscatter signal $S_{R\to T\to R}$. Suppose the transmitted signal of reader is

$$S_R(t) = v \cdot \cos(2\pi ft - \phi_R) + u \cdot \sin(2\pi ft - \phi_R) \tag{4}$$

where u and v denote the unit vectors of the reader's two orthogonal polarized directions, ϕ_R denotes the phase shift induced by reader circuits, and f is the communication frequency.

Then, we can model the tag's received signal as

$$\begin{aligned} S_{R\to T}(t) &= p \cdot S_R(t - t_{R\to T} - t_T) + q \cdot S_R(t - t_{R\to T} - t_T) \\ &= |p| \cos(2\pi ft - \phi_R - \phi_d - \phi_T - \alpha) \\ &\quad + |q| \sin(2\pi ft - \phi_R - \phi_d - \phi_T - \alpha) \\ &= \sqrt{p^2 + q^2} \cos\left(2\pi ft - \phi_R - \phi_d - \phi_T - \alpha - \arctan\frac{q}{p}\right) \end{aligned} \tag{5}$$

where q and p denote the unit vectors of the tag's two orthogonal polarized directions (q does not exist for linearly polarized tag), and ϕ_d and ϕ_T denote the phase shifts induced by reader–tag distance and tag hardware, respectively. α is the intersection angle between v and p.

Accordingly, the tag's LOS backscatter signal received by the reader can be described as

$$\begin{aligned} &S_{R\to T\to R}(t) \\ &= \sqrt{p^2 + q^2} \cos\left(2\pi ft - 2\phi_d - \phi_R - \phi_T - 2\alpha - \arctan\frac{q}{p}\right) \end{aligned} \tag{6}$$

and the total phase shift is $\phi = 2\phi_d + \phi_R + \phi_T + 2\alpha + \arctan\frac{q}{p}$.

Based on this, we can get two properties of $S_{R\to T\to R}$ if we spin the reader antenna around its center, in a fixed spinning plane orthogonal to the spinning shaft.

1) *Linearity of Phase Changes:* When spinning the reader antenna with a uniform speed, the intersection angle α and thus the phase shift ϕ would change linearly.
2) *Stability of RSS:* The amplitude of the LOS signal should not change with α. Hence, the RSS would remain stable when spinning the antenna.

To verify the above properties, we conduct empirical studies using a COTS ImpinJ R420 reader [22] and tags with three different models (AZ9662, H47, and L27D) in an open area with wave-absorbing material deployed. Fig. 5 demonstrates that the two properties are applicable to various tag models, even if their polarization types are different. This also indicates that our proposed phase model is more universal and advanced than past ones [25], [26].

Next, we consider the practical effects of multipath signals (e.g., $S_{R\to T\to O_1\to R}$) reflected by surrounding obstacles. The

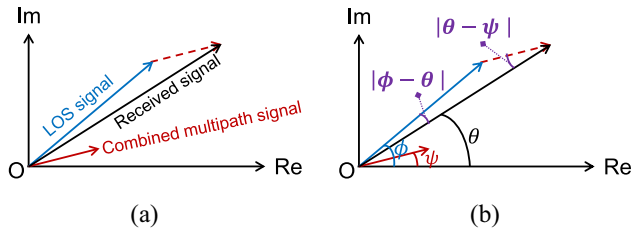

Fig. 6. Multipath effect on LOS signal. (a) Superposition of signals. (b) Phase shifts' relationship.

combination of multipath signals can be approximated as

$$S_M(t) \approx \sum_{i=1}^{N} \left(S_{R\to O_i\to T\to R}(t) + S_{R\to T\to O_i\to R}(t)\right) = \sum_{i=1}^{N} 2\sqrt{p^2+q^2}\eta_i \cos(\beta_i-\alpha)\cos(2\pi ft-\delta_i) \quad (7)$$

where $\delta_i = 2\phi_{RO_iTR} + \phi_R + \phi_T + \phi_{O_i} + \alpha + \beta_i + \arctan(q/p)$. η_i is the attenuation coefficient of obstacle O_i and β_i is the intersection angle between main direction of O_i and p. ϕ_{RO_iTR} and ϕ_{O_i} refer to the phase shifts induced by the distance of the ith propagation path and reflection of O_i, respectively. The signals after multi-reflections can be negligible due to the large amplitude attenuation, as compared to the LOS signal.

The RSS and phase readings reported by a commercial reader (denoted by P and θ) are collected from the superposition of the LOS signal and combined multipath signal [see Fig. 6(b)]. So we can obtain the following relationships:

$$|\phi-\theta| = \arcsin\left(\sqrt{\frac{P_M}{P}}\sin|\phi-\psi|\right) \quad (8)$$

$$\sqrt{\frac{P_{\text{LOS}}}{P}} = \frac{\sin(\theta-\psi)}{\sin(\phi-\psi)}. \quad (9)$$

Here, P_{LOS} and P_M denote the RSS of the LOS signal and multipath signal, respectively, ψ denotes the combined multipath signal phase. From (7), we can prove that both P_M and ψ change nonlinearly with α (see the Appendix). P_M also changes nonmonotonically. Besides, their changing tendencies in one period are evidently inconsistent. Thus, $|\phi-\theta|$ would change nonlinearly and nonmonotonically likewise when spinning the antenna, in terms of (8). Further, $\sin(\theta-\psi)/\sin(\phi-\psi)$ in (9) would also fluctuate within a small range around 1, incurring the instability of P. Therefore, we can exploit our proposed two properties of the LOS signal: *linearity of phase changes* and *stability of RSS* to alleviate multipath reflections' impacts and refine ϕ. The specific procedure is elaborated in the following sections.

B. Phase Vector Regression

We first consider the fixed-interval spinning scenario, i.e., spinning the reader antenna with a fixed step of $\Delta\alpha$ and collecting signal features at each spinning angle.

After antenna spinning and phase unwrapping based on the monotonicity, we can obtain a vector of average phases $\Theta = \{\hat{\theta}_1, \hat{\theta}_2, \ldots, \hat{\theta}_M\}$, where $\hat{\theta}_k$ is the average phase at the kth spinning angle and M is spinning angles' quantity. Then, we utilize the linear regression method to fit Θ into a line, whose gradient is a known constant $2\Delta\alpha$ in terms of (6)

$$b^* = \arg\min_b \sum_{k=1}^{M} \omega_k \cdot \left(2\Delta\alpha\cdot k + b - \hat{\theta}_k\right)^2 = \sum_{k=1}^{M} \omega_k \cdot \left(\hat{\theta}_k - 2\Delta\alpha\cdot k\right) \quad (10)$$

where b^* denotes the intercept of the fitting line. ω_k is a weight reflecting the confidence level of $\hat{\theta}_k$, specifically defined as

$$\omega_k = \mu_k / \sum_{L=1}^{M}\mu_L, \quad \mu_k = 1 - \frac{1}{2\pi}\sqrt{\sum_{j=1}^{U_k}\left(\theta_{k,j}-\hat{\theta}_k\right)^2/U_k} \quad (11)$$

where U_k and $\theta_{k,j}$ denote the reading times and unwrapped phase of the jth reading, respectively, at the kth spinning angle. This means that the spinning angle with a smaller phase variance would be assigned a larger weight in linear regression. This is reasonable since smaller phase variance reflects cleaner signal features collected at this angle.

After the regression, we can greatly alleviate multipath effects due to the first property in Section III-A, whereas the obtained intercept b^* could still contain some drift incurred by uncertain environmental noises. Next, we utilize RSS for further refinement.

C. Intercept Drift Calibration

After spinning antenna, we can also obtain a vector of average RSS $\Upsilon = \{\hat{P}_1, \hat{P}_2, \ldots, \hat{P}_M\}$. Then, we consider to match the phase error with the RSS error at the same angle and thus calibrate the possible intercept drift Δb (within an empirical threshold ϵ), according to the second property in Section III-A and the consistency in Section II. That is

$$\Delta b^* = \arg\min_{-\varepsilon\le\Delta b\le\varepsilon} \max_{1\le k\le M} \left\{ \frac{\left|2\Delta\alpha\cdot k + b^* + \Delta b - \hat{\theta}_k\right|}{\left|\hat{P}_k - \sum_{L=1}^{M}\gamma_L\hat{P}_L\right|^{\sigma}} \right\} \quad (12)$$

where σ is an empirical parameter for normalization and γ_k is a weight reflecting the confidence level of $\hat{P}_k$, defined as

$$\gamma_k = \tilde{\mu}_k / \sum_{L=1}^{M}\tilde{\mu}_L, \quad \tilde{\mu}_k = 1 - \sqrt{\sum_{j=1}^{U_k}\left(P_{k,j}-\hat{P}_k\right)^2/U_k} \quad (13)$$

where $P_{k,j}$ denotes the reported RSS of the jth reading at the kth spinning angle. This means the spinning angle with a smaller RSS variance would be assigned a larger weight in the calculation of average Υ. We can transform (12) into another formulation

$$\begin{aligned} \Delta b^* = \ & \arg\min_{\zeta\ge 0} \zeta \\ \text{s.t.} \quad & -\varepsilon \le \Delta b \le \varepsilon \\ & -\zeta \le \frac{2\Delta\alpha\cdot k + b^* + \Delta b - \hat{\theta}_k}{\left(P_k - \sum_{k=1}^{M}\gamma_k P_k\right)^{\sigma}} \le \zeta, \forall k \end{aligned} \quad (14)$$

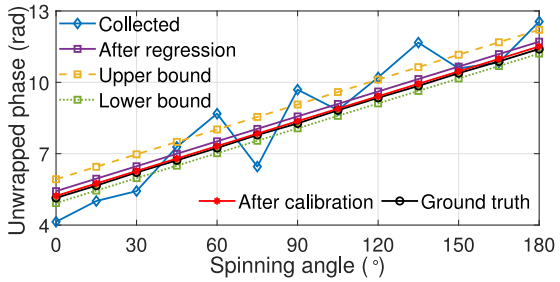

Fig. 7. LOS signal phase refinement under multipaths.

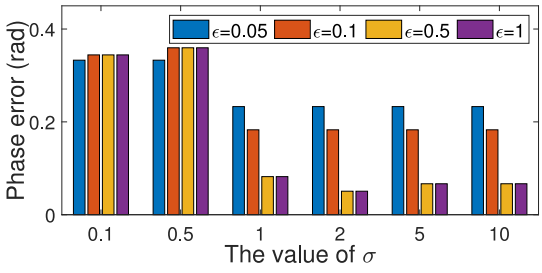

Fig. 8. Refined phase error versus (ϵ, σ).

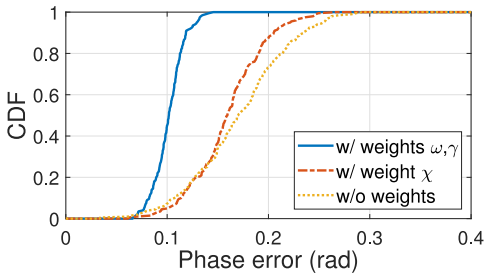

Fig. 9. Refined phase error under different weights.

where Δb and ζ are variables to optimize. Afterward, we can solve (14) using the linear programming (LP) method and obtain Δb^*.

After the calibration, $2\Delta\alpha \cdot k + b^* + \Delta b^*$ is treated as the refined phase shift of LOS signal at the kth spinning angle and inputted to existing RFID sensing systems. Here, we illustrate an example in Fig. 7, where the ground truth of LOS signal phases is obtained in the same environment as Fig. 5, and we deploy some obstacles around to construct a multipath-prevalent scenario and collect the phase readings. We can find that the maximum difference between collected phase and ground truth reaches 1.820 rad, but degraded to only 0.308 rad after phase vector regression. By intercept drift calibration, the difference is further reduced to $\leq$0.107 rad. These results all demonstrate the potency of our method and many RFID sensing systems can benefit from it. Taking object localization as an instance, if the phase measurement error can be reduced from 1.820 to 0.107 rad, the distance error could be declined by nearly 20×.

Besides, we study the effects of empirical parameters ϵ and σ, respectively. As sketched in Fig. 8, on the one hand, the phase error decreases initially with the increasing σ and grows later when $\sigma \geq 5$. This is reasonable because a small σ may degrade the capability of intercept drift calibration whereas a large σ may overly rely on the function of RSS. Only a moderate σ can achieve the optimal performance. On the other hand, very small ϵ yields limitations for the available range of Δb and the performance is basically stable when $\epsilon > 0.5$ because the optimal Δb may probably be found within a range of $\epsilon \leq 0.5$. Therefore, we recommend users to choose $\sigma \in [1, 2]$ and $\epsilon \in [0.4, 0.6]$ for better performance.

In addition, we investigate the effect of used weights ω and γ in our scheme. From Fig. 9, we can find that even though our scheme can work without the weights (i.e., weight values equal to each other), leveraging the weights can help reduce the median error of the refined phase by 0.069 rad.

D. Real-Time Spinning

Next, we extend our scheme to the real-time spinning scenario with a constant spinning speed v_s. Different from fixed-interval spinning, the step $\Delta\alpha$ is not a constant because the commodity tags adopt the random backoff mechanism [27] and thus the readings of signal features are not uniform. Due to this "nonuniform sampling" phenomenon, our above scheme cannot directly apply to the real-time spinning scenario. Fortunately, the arrival time of the backscatter signal (i.e., timestamp) is reported by the COTS reader for each sample. Let $\Xi = \{\tau_1, \tau_2, \ldots, \tau_M\}$ denote the timestamps of M collected samples and τ_0 denote the starting time of spinning. The corresponding spinning angle of the kth sample is $v_s \cdot (\tau_k - \tau_0)$.

However, there remains another problem: the weights in Sections III-B and III-C need multiple samples (at least two samples) for calculation. For a single sample, it is hard to measure the confidence level of phase and RSS. Otherwise, the regression and calibration without weights probably incur performance loss. Here, we develop DFS to address it, according to the consistency in Section II. We divide DFS values into 11 ranks: $|F_m| \leq 10$, $10 < |F_m| \leq 20$, $20 < |F_m| \leq 30$, …, $90 < |F_m| \leq 100$, $|F_m| > 100$, and the corresponding weights are 1, 0.9, 0.8, …, 0.1, 0.

Then, the procedure of phase vector regression could be modified as

$$b^* = \sum_{k=1}^{M} \chi_k \cdot \left(\hat{\theta}_k - 2v_s \cdot (\tau_k - \tau_0)\right) \tag{15}$$

where χ_k is the weight of the kth angle derived from DFS rank.

Similarly, by leveraging the same weight χ_k, the procedure of intercept drift calibration could be modified as

$$\Delta b^* = \arg\min_{-\varepsilon \leq \Delta b \leq \varepsilon} \max_{1 \leq k \leq M} \left\{ \frac{\left|2v_s \cdot (\tau_k - \tau_0) + b^* + \Delta b - \hat{\theta}_k\right|}{\left|\hat{P}_k - \sum_{L=1}^{M} \chi_k \hat{P}_L\right|^{\sigma}} \right\} \tag{16}$$

and we can use the LP method to solve it likewise.

To verify the function of χ, we exploit DFS readings collected from experiments in Fig. 7 to compute DFS-based weight χ. Then, we use χ to obtain the refined phase, instead

of the weights ω and γ. Fig. 9 gives the performance comparison between different weights. Compared to the result without any weights, using χ can reduce the median error of the refined phase by 0.011 rad. However, it cannot reach the performance of using ω and γ, with 0.058 rad disparity. Actually, the performance loss from fixed-interval spinning to real-time spinning inevitably exists. Besides weight factor, the possible speed error [denoted by $\rho(\nu_s)$] also increases the refined phase error. To specifically measure how much performance loss from fixed-interval spinning to real-time spinning, below we calculate the theoretical error gap between them. If the error gap is bounded by a threshold, we can thus infer the performance of real-time performance from that of fixed-interval performance.

First, the error of spinning angle is $|\rho(\nu_s)\cdot(\tau_k-\tau_0)|$ for the kth sample and that of b^* is $|\rho(\nu_s)\cdot 2\sum_{k=1}^{M}\chi_k(\tau_k-\tau_0)|$ in terms of (15). Accordingly, the phase error gap after regression is totally $|2\rho(\nu_s)(\tau_M-\tau_0)+2\rho(\nu_s)\sum_{k=1}^{M}\chi_k(\tau_k-\tau_0)|$, which is less than $|2\rho(\nu_s)((\tau_M-\tau_0)+\sum_{k=1}^{M}(\tau_k-\tau_0))|$ since the weight satisfies $\chi_k\le 1,\ \forall k$. Second, the phase error gap can be described as $|2(\rho(\nu_s)/\nu_s)\cdot\nu_s((\tau_M-\tau_0)+\sum_{k=1}^{M}(\tau_k-\tau_0))|\le 2|\rho(\nu_s)/\nu_s|\cdot|\nu_s((\tau_M-\tau_0)+\sum_{k=1}^{M}(\tau_k-\tau_0))|$, where $(\rho(\nu_s)/\nu_s)$ is the relative error of spinning speed. Due to that one-round spinning is sufficient for our scheme, we have $|\nu_s(\tau_M-\tau_0)|\le 2\pi$. Thus, $|\nu_s((\tau_M-\tau_0)+\sum_{k=1}^{M}(\tau_k-\tau_0))|\le 2(M+1)\pi$ because of $\tau_k\le\tau_M,\forall k$. Accordingly, the phase error gap after regression is less than $4\pi(M+1)|\rho(\nu_s)/\nu_s|$. Third, the calibration would decrease the error gap, since using the LP method can find the globally optimal Δb^* and $\Delta b=0$ is one of the feasible solutions. Using the proof by contradiction, the conclusion can be readily derived.

Therefore, the error gap of refined phase between real-time spinning and fixed-interval spinning would not exceed $4\pi(M+1)|\rho(\nu_s)/\nu_s|$. That is, the theoretically upper bound of performance loss is $4\pi(M+1)|\rho(\nu_s)/\nu_s|$ for real-time spinning as compared to fixed-interval spinning. For example, if the relative error of spinning speed is 0.1% and the samples' quantities are 12, the upper bound is 0.163 rad which is acceptable for most applications. By selecting an efficient electric shaft to decrease $|\rho(\nu_s)/\nu_s|$ and accelerating the spinning/declining the sampling rate to decrease the collected samples' quantities M, the upper bound can be further reduced.

E. Practical Issues

We discuss some issues to deploy RoSense in practical RFID applications from four aspects.

Feasibility: The size and weight of a spin shaft are much smaller than a commercial RFID reader antenna, with little impact on equipment setup. Also, a spin shaft is not costly as compared to RFID infrastructures. Besides, the reader antenna is always deployed on the ceiling in the industrial IoT environment such as warehouse [9]. The spinning antenna is far from people working in the area, with little risk of injury. Reference [28] also spins the reader antenna and verifies the feasibility.

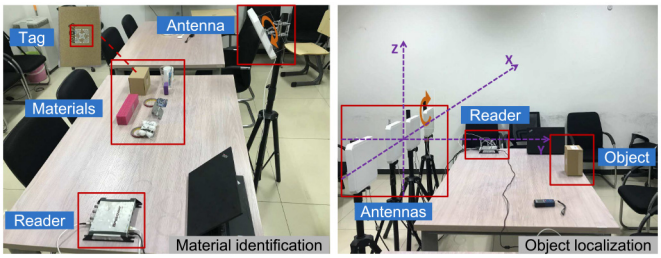

Fig. 10. Experimental setup for two cases of RFID sensing.

3-D Scene: The signal propagation, including LOS and multipaths, takes place in 3-D space and RoSense is applicable to 3-D scenes. We should emphasize that our method does not require the RFID tag and the reader antenna to be perfectly aligned (see our experiment setup in Section IV). As long as the spinning plane of the reader antenna is fixed, two properties of the LOS signal will hold and RoSense can work.

Ubiquity: We should emphasize the difference between customized RF devices and our mechanical spin axis. The disadvantages of customized RF devices like USRP contain not only extra device costs but also the incompatibility with existing RFID infrastructure and low ubiquity for numerous RFID applications. As mentioned in [2], non-commodity RF products make a slow adoption and complex deployment. This is recognized by the research community on RFID sensing [12]. Different from that, a mechanical spin axis is COTS, common to find and nonintrusive. Wang *et al.* [28] also indicated this point. So we think our method is much more ubiquitous.

Application Scope: Though environmental reflections are the most common multipath phenomena that RoSense mainly focuses on, RoSense can always work as long as the LOS signal exists, no matter the circumstances are reflections or diffractions because the basic idea of RoSense is to exploit two properties of LOS signal during antenna spinning. Despite this, if the LOS signal is nonexistent (e.g., blocked by obstacles), our method will also lose efficacy. Moreover, similar to CPIX [17], RoSense is aimed at sensing cases with stationary tags (e.g., localization) and cannot be directly applied to moving tags' cases (e.g., tracking) due to the spinning latency. We will take further studies to extend the application scope of RoSense in our future work.

IV. System Implementation

We implement a prototype of RoSense with COTS devices and evaluate it in two cases: 1) nonintrusive material identification using Tagtag [3] and 2) anchor-free object localization using BackPos [1]. The employed hardware contains one ImpinJ Speedway R420 RFID reader with E9028PCRNF/Laird S9028PCL/Alien ALR8698 antennas [23], [29] and Alien AZ-9662/ImpinJ H47/ImpinJ L27D tags [22], [23], all operating at the UHF band of 920.625–924.375 MHz. The reader is connected to our ThinkPad L490 laptop (i7-8565U CPU and 16G memory) through low-level reader protocol (LLRP) [30]. The software, including signal features collection and our algorithms for phase refinement, is implemented using Java and MATLAB.

The experimental setup for two cases is shown in Fig. 10, where the ground truth of object localization is measured using a laser range finder and that of material identification is labeled in advance. A commodity mechanical spin shaft on the antenna holder is used for spinning the reader antenna. Here, we only implement the fixed-interval spinning since the performance loss of real-time spinning is bounded and we can infer it from the performance of fixed-interval spinning. At each spinning angle, we collect signal features for no more than 1 s. After the procedure of RoSense, the refined phases of all antennas at the same initial angle are inputted to BackPos and Tagtag for sensing, if more than one antenna is employed (generally BackPos requires four antennas).

For comparison, we also implement the state-of-the-art work CPIX [17] and baseline scheme (i.e., using original unrefined phases as inputs) on BackPos and Tagtag, respectively. Below we introduce the details of them.

Tagtag [3]: From phase readings before/after a tag is attached to the target, we can extract impedance-related phase change as the material pattern. Besides, by using RSS and frequency channel hopping, the effects of tag–reader distance and rotations can be removed. Finally, we compare the material pattern with the fingerprint database and thus identify the target's material type.

BackPos [1]: For every two antennas, the differential phase can reflect the distance gap between two tag–antenna pairs, and thus a hyperbola can be obtained. The intersections of each three hyperbolas are the candidates of the tag's location. By using four antennas, we can construct two groups of intersections and find the nearest two points. Finally, the average location of these two points is regarded as the localization result.

CPIX [17]: This is a method to cleanse the phase. We employ the reader to exploit frequency channel hopping with a step of 0.25 MHz and collect signal features on 16 channels. By fitting the collected phases on all channels into a straight line, the obtained phase on each channel is regarded as the cleansed phase.

The specific evaluation and in-depth discussions are presented in the following section.

V. Evaluation

We conduct the performance evaluation of RoSense in our lab environment (see Fig. 10). Besides the overall performance, we also study the impacts of environmental factors, device conditions, and reader configurations on our method to examine the robustness.

A. Case I (Material Identification)

We choose ten different types of materials for experiments, whereas it is hard to receive signals when tagged on metal and liquid materials, and only six types of them are applicable: 1) carton; 2) foam; 3) cotton; 4) ceramic; 5) glass; and 6) plastic. Fig. 11 shows the average identification accuracy of each material. We can find that Tagtag is vulnerable to multipaths and its accuracy would drop down to 70.71%. RoSense can improve the overall accuracy by 11.74% (relatively 16.22%),

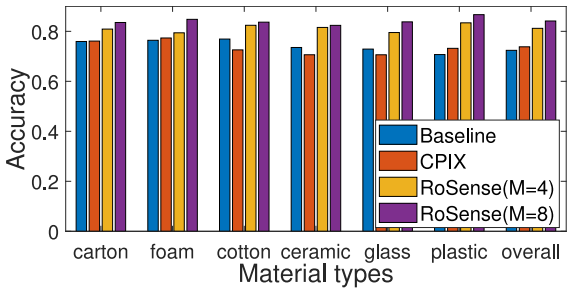

Fig. 11. Performance of material identification.

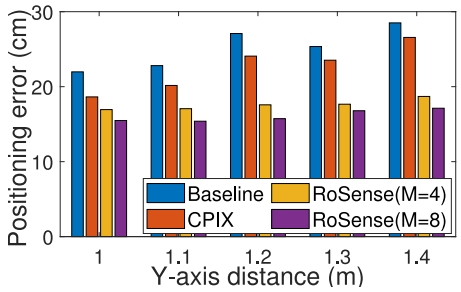

Fig. 12. Performance of object localization.

greatly outperforming CPIX by 8.3×. Besides, RoSense is available for all materials and CPIX would even impair the performance in ceramic and glass cases. There are probably two reasons: 1) the phase shift may not regularly change with frequency channels when tags are bent (e.g., tagged on a glass cup) and 2) the phase cleansing procedure of CPIX is coarse without mechanism support. Among all materials, the accuracy improvement of RoSense can reach 15.96% and that of CPIX is up to 2.49%, which indicates the significant superiority of RoSense. Moreover, a larger number of spinning angles M could further promote the performance to a certain degree. For instance, spinning eight angles ($\Delta\alpha = 45°$) can achieve higher accuracy than that of spinning four angles ($\Delta\alpha = 90°$) by 2.94%. This is reasonable since more angles would engender more precise regression and calibration. Fig. 13(a) demonstrates that one material features at a certain channel under terrible multipaths. We can see that the evident variance can reach 4.268 rad within the 2π range, and it can be reduced by 72.21% using RoSense and only 21.33% using CPIX. Actually, the variance using CPIX only descends to 3.357 rad and the material feature is still not stable. Therefore, it is much more effective to use RoSense for phase refinement as compared to CPIX.

B. Case II (Object Localization)

We leverage four reader antennas with known coordinates for object localization, where the y-axis distance from antenna to tag is fixed in each experiment. BackPos is used to compute the tag's X- and Z-coordinates and obtain the positioning error. From Fig. 12, we can find that BackPos's mean error can be enlarged up to 28.51 cm under multipaths. Our method RoSense can help reduce the positioning error to 17.12 cm. As compared to CPIX, RoSense can achieve a much larger reduction of error by nearly 5.9×. Besides, RoSense maintains

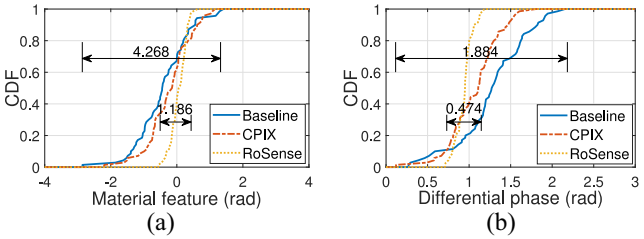

Fig. 13. Experimental results of material feature and differential phase. (a) Material feature distribution on one channel. (b) Differential phase distribution of two antennas.

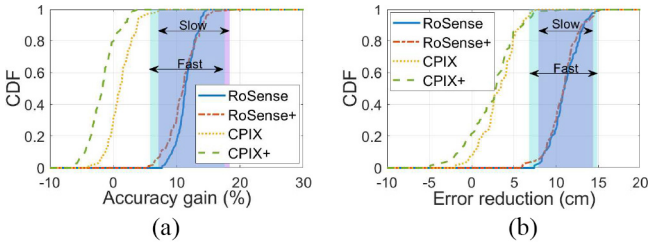

Fig. 14. Performance under environments w/o and w/ human mobility. (a) Distribution of material identification accuracy gain. (b) Distribution of positioning error reduction.

a high performance under different y-axis distances, whereas the effect of CPIX is attenuated with the increasing distance, probably due to that larger distance incurs a worse fitting error in CPIX. This also proves that RoSense can work effectively wherever the tag is located, but CPIX fails. Further, Fig. 13(b) reveals a distribution of two antennas' differential phase at a certain position. We can notice that RoSense helps reduce the wide variance of differential phase by 74.84%, whereas the reduction using CPIX is only 10.52%. Moreover, there exists a certain possibility that CPIX may enlarge the variance instead. Hence, using RoSense is much more reliable.

C. Impact of Environments With Human Mobility

Like [17], we evaluate the robustness of our method in the environment with human mobility. To construct such an environment, we let a person randomly walk nearby our setup. Fig. 14 shows the accuracy gain of material identification and error reduction of object localization (as compared to baseline schemes), where the sign with or without "+" means whether the evaluation is under human mobility or not. We can have two observations. On the one hand, RoSense can always benefit the sensing performance (e.g., by 5.07–12.19 cm for localization). The positioning errors using RoSense can even approach the results measured in a low multipath environment. On the other hand, the CDF curves of RoSense and RoSense+ are similar to each other. For example, the probability of over 10 cm localization error reduction under human mobility is around 70.0%, only with a 4.3% drop from that under no human mobility. Meanwhile, the results of CPIX evidently stray away from each other. Even worse, CPIX under human mobility may impair the performance for some samples, in both material identification and object localization. This indicates that RoSense is more robust to human mobility as compared to CPIX. That is, RoSense can work under

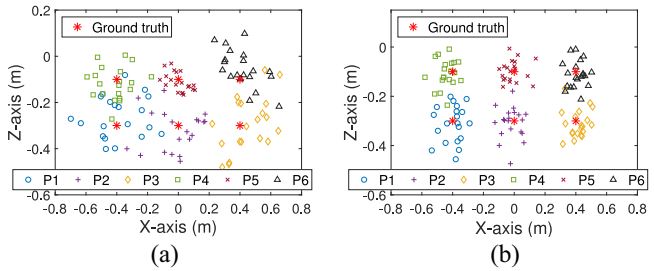

Fig. 15. Localization results under different deployment angles (different positions). (a) Positioning using baseline scheme. (b) Positioning using RoSense.

both stationary and mobile multipaths. In addition, we can find that though the person's walking speed determines mobile multipath conditions, it does not affect the performance of RoSense as long as the LOS signal exists. This also indicates the versatility of RoSense under different multipath conditions.

D. Impact of Deployment Angle

As mentioned in [10], when the tag situates at different positions in the receiving beam of the reader antenna, the corresponding "deployment angle" is different and may affect the sensing performance. So we change the tag's position along the x-axis and z-axis for evaluation, where the zero points of the x-axis and z-axis refer to the antennas' midpoint and height, respectively. Fig. 15 shows the obtained localization results in the X–Z plane. In Fig. 15(a), we can find that the localization error is smaller on the positions closer to the center, i.e., smaller deployment angle. For example, the mean error of point $(0, -0.3)$ is 9.21 cm less than that of point $(-0.4, -0.3)$. Also, the mean error of point $(-0.4, -0.3)$ is similar to that of $(0.4, -0.3)$ due to the symmetry, i.e., the same deployment angle. This phenomenon reveals that the multipath conditions at different deployment angles are different and a large deployment angle probably incurs more severe multipaths. After the procedure of RoSense in Fig. 15(b), the messy localization results become to gather nearby the ground truth. Besides, the localization error on the edge is reduced to approach the error on the center, e.g., the gap between the mean error of point $(-0.4, -0.3)$ and point $(0, -0.3)$ is only 1.24 cm. Actually, the error reduction on the edge is more evident than that on the center. To summarize, by leveraging RoSense, we can localize the tags at different deployment angles with high precision.

E. Impact of Device Diversity

Device diversity is also a critical factor affecting the signal phase [31]. First, we examine the effect of RoSense on three tag models with different polarization types (see Fig. 16). Note that these three polarization types can cover almost all tags' polarization types [24] and the working mechanism of our method is based on tags' inherent polarization properties (see Section III-A). Accordingly, the sensing performance on these three tag models can testify to the universality of RoSense to a large extent. From Table I, we can observe that RoSense can achieve fine performance gain on all tag models. The gain on

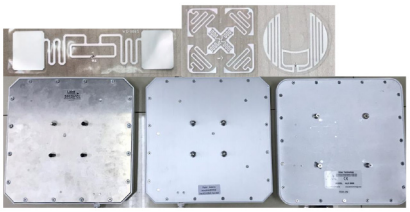

Fig. 16. Tested devices.

TABLE I
PERFORMANCE ON DIFFERENT TAG TYPES

Tag Model	Material Identification	Object Localization
AZ9662	↑ 8.25% accuracy	↓ 10.36cm error
H47	↑ 11.74% accuracy	↓ 11.38cm error
L27D	↑ 5.86% accuracy	↓ 7.54cm error

TABLE II
PERFORMANCE ON DIFFERENT READER ANTENNA TYPES

Antenna Model	Material Identification	Object Localization
E9028PCRNF	↑ 11.74% accuracy	↓ 11.38cm error
Laird S9028PCL	↑ 9.53% accuracy	↓ 12.22cm error
Alien ALR8698	↑ 11.26% accuracy	↓ 11.95cm error

linearly polarized (AZ9662) or dual-linearly polarized (H47) tags is a little larger than that on circularly polarized (L27D) tags. For example, the mean reduction of localization error on H47 tags is 3.84 cm greater than that on L27D tags. This is probably because the communication capability of circularly polarized tags is lower than the others. Then, we fix the tag model H47 and evaluate RoSense on three reader antenna models. This article only considers the common reader antenna models which are circularly polarized [24], and these three antennas are typical ones. Table II gives the results. We notice that the performance gap between different antenna models is slight, e.g., only 0.84 cm in localization. This is reasonable since whatever the antenna type is, the hardware noise would not affect the two properties leveraged in RoSense. Besides, the algorithms in Tagtag and BackPos have removed a part of the devices' impact. In summary, our method is universal for diverse tags and reader antennas.

F. Impact of Tag's Orientation

Below we evaluate the effect of the tag's orientation. Fig. 17(a) demonstrates the CDF curves of localization error reduction under distinct tag's orientation 0°, 45°, 90°, and 180°. We can find that the CDF curves are very close to each other, where the mean error reduction is 11.09, 11.66, 11.15, and 11.40 cm. This is reasonable since our two properties in Section III-A are independent of the tag's orientation. In practice, the phase is determined by the relative orientation of the tag and reader antenna. When spinning the reader antenna over 2π angles, only the sequence of phase vectors will translate with the tag's orientation. The sequence translation of elements in phase vector regression will not affect the fitting result. Therefore, RoSense can work regardless of the tag's orientation.

G. Impact of Frequency Channel

We evaluate RoSense under four frequency channels from 921 to 924 MHz. As shown in Fig. 17(b), the mean localization error reduction on 922 MHz is the largest (12.61 cm) while that on 923 MHz is the smallest (9.35 cm). RoSense exhibits various performance gains on different channels, though RoSense seems to be independent of channels. The main reason is that on different frequency channels, the multipath effects are distinct due to the signal superposition. The practical errors of the collected phase and RSS rely on both the time- and frequency-domain, when the LOS signal combines with multipath signals. The phase deviation is possibly large on some channels and small on the others. This also conforms to the conclusion in CPIX. Consequently, on different channels, the error reduction degrees using our algorithms are diverse. Despite all this, RoSense can greatly benefit the localization performance whatever the used channel is.

H. Impact of Transmission Power

Higher levels of transmission power lead to a larger receiving beam of reader antenna and also higher possibilities of severe multipaths. We adjust the transmission power from 24 to 30 dBm and Fig. 17(c) shows the corresponding localization results. The error reduction using 30 dBm is 4.27 cm greater than that using 24 dBm. This is probably because when the power level increases, the baseline scheme's localization error may also be magnified. It also indicates that RoSense can maintain a fine capability to refine the phase, even using a large transmission power with severe multipaths.

I. Impact of Reader Modes

In the reader configurations, there mainly exist four reader modes: MaxThroughput, Hybrid, DenseReaderM4, and DenseReaderM8, which correspond to four encoding forms: FM0, Miller2, Miller4, and Miller8 [32]. Provided that BLF is fixed (e.g., 170.6 kHz using the reader of the FCC version), the data rate (the number of queries per second) is determined by the encoding forms, e.g., 170.6/8 = 21.32 b/s of Miller8 and 170.6/4 = 42.65 b/s of Miller4. FM0 has the highest data rate. However, generally a high data rate would bring low robustness to environmental interference. In our above experiments, the default encoding form is FM0. We change the encoding forms and Fig. 17(d) depicts the corresponding results of localization error reduction, which verifies the feasibility of RoSense under diverse reader modes though with varying error reduction degrees.

Besides, we get one critical observation through experiments: the half-wave loss will vanish only if FM0 mode is used. That is, using the other three modes, the collected phase always has a π deviation which is incurred by reader firmware (not multipaths). So, we recommend using the FM0 mode instead of the other modes since RoSense itself can refine the sensing performance against multipaths.

In addition, different data rates lead to different packet duration ΔT in (3) and thus different DFS. In the above experiments, the default weights used in phase vector regression and intercept drift calibration are ω and γ. Below

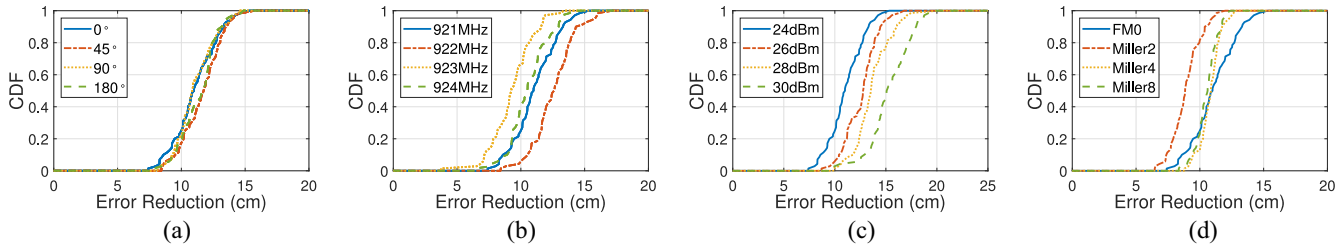

Fig. 17. Robustness evaluation of RoSense under different environmental settings and reader configurations. (a) Error reduction versus tag's orientation. (b) Error reduction versus channel. (c) Error reduction versus power. (d) Error reduction versus encoding form.

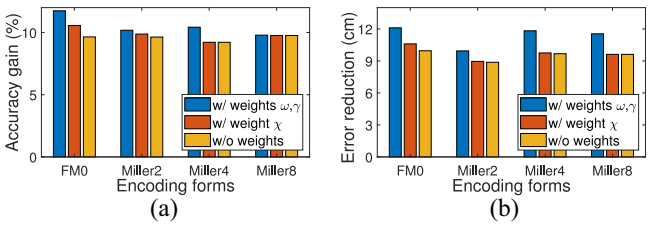

Fig. 18. Performance under different weights. (a) Accuracy gain versus weights. (b) Error reduction versus weights.

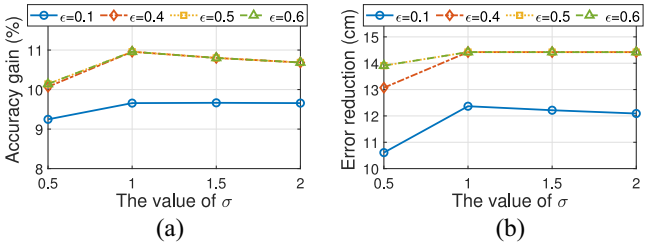

Fig. 19. Performance under different parameters ϵ and σ. (a) Accuracy gain versus ϵ and σ. (b) Error reduction versus ϵ and σ.

we study the effect of different weights as described in Section III-D. Fig. 18 shows the performance gain under different weights. On the one hand, our default weights achieve the best performance for both material identification and object localization. This indicates the effectiveness of our weights. On the other hand, for Miller encoding, the performance gain using weight χ nearly approaches that without any weights. This is probably due to coarse-grained DFS ranks. When using Miller encoding instead of FM0, the ΔT becomes larger and thus the DFS value decreases in terms of (3) for the same $\Delta\phi$. For example, all DFS values are lower than 10 Hz using Miller encoding and accordingly the weight χ loses its effect. So we recommend making more fine-grained DFS ranks. Actually, both very low and high data rates would not be suitable for weight χ. Low data rates yield very small DFS values and the DFS-weight translation is not convenient. On the contrary, large DFS values may increase the risk that one sample's DFS is easily interfered during such a short ΔT, yielding DFS unable to correctly reflect the multipath conditions. Hence, when manipulating real-time spinning, we suggest calculating the results not only with weight χ but without any weights. By comparing their similarity, a more reliable result could be obtained. These conclusions would not affect the performance in fixed-interval spinning since using our default weights is adequate.

J. Impact of Parameter Values ϵ and σ

In the end, we measure the impact of parameter values ϵ and σ used in Section III-C. As stated above, we recommend to choose $\sigma \in [1, 2]$ and $\epsilon \in [0.4, 0.6]$, which conforms to the results in Fig. 19. When ϵ and σ are situated in our given intervals, we can achieve the peak performance with very slight variance. But when $\sigma = 0.5$, the performance degrades by 0.89% in accuracy improvement of material identification and 1.35 cm in an error reduction of localization. If $\epsilon = 0.1$, the accuracy would be further declined by 1.71% at most, and similarly the error would be raised by 3.81 cm. Therefore, inappropriate parameter values may weaken the capability of RoSense.

Through all experiments in Section V, we verify that our method RoSense is universal and effective to enhance the RFID sensing performance under multipaths.

VI. Related Work

RFID Sensing: Due to the small-sized, low-cost, label-capability, and battery-free advantages of passive tags, RFID sensing grows to become one of the promising wireless sensing techniques. Recent works have exploited RFID sensing in masses of IoT applications, e.g., object localization [1], [4], [33], vibration inspection [6], [7], [34], material identification [3], [23], [35], orientation detection [36], [37], temperature monitoring [10], [38], wetness sensing [39], [40], and items anti-counterfeiting [31], [41]. As one of the vital signal features provided by COTS readers, the phase shift is commonly used in RFID sensing systems and is always superior to other features like RSS because of its fine granularity [10].

Multipath Effect: Environmental multipath reflection is an inherent phenomenon, which however significantly limits the RFID sensing performance [17]. There are two reasons. First, COTS readers can only report limited features of backscatter signals. If the LOS signal is superposed with multipath signals, the signal amplitude and phase would be severely influenced, making the sensing results inaccurate. Second, UHF RFID applications with finite communication distance are mainly deployed in the indoor environment and the multipath effect is inevitable and common to happen. However, most past works neglect this problem by simply choosing a clean channel for communication [3], [25].

Phase Refinement Against Multipaths: Existing works to deal with mulitpaths mostly rely on customized software-defined radios like USRP [14], [35]. The rest consider offline training to learn multipath profiles [15], [16], which needs a lot of human efforts and is inapplicable to a new environment yet. In addition, some works exploit differential phases of two tag–antenna links [1], [8] and reckon the attenuation of multipath effect, which practically makes little progress. The only work especially focusing on multipath and able to cleanse the signal phase is CPIX [17]. It leverages frequency channel characteristics to improve the sensing performance to a certain degree. Despite this, CPIX has a few shortages. On the one hand, the performance gain using CPIX is volatile. For example, the antenna coupling and environmental noise change with different channels. Our experiments in Section V also verify that CPIX may even degrade the sensing performance in some cases. On the other hand, the time delay of CPIX is high and thus not applicable to real-time applications. Therefore, there still lacks an effective and universal solution to address the problem of multipaths, with purely COTS devices.

Antenna Spinning: Different from tag's rotation sensing [6], [25], [42], few works consider to spin the reader antenna. To our knowledge, Spin-Antenna [28] is the only work to use a spinning antenna to track the 3-D motion of a specified object attached with a tag array. Though its purpose and used method entirely different from ours, it verifies the feasibility of implementing a spinning antenna. Among the past works, none of them explore the specific relationship between the antenna spinning and multipath effect.

Our method RoSense is the first attempt to exploit the phase and RSS vectors through antenna spinning to refine the LOS signal phase under multipaths. Instead of channel hopping in CPIX, antenna spinning would lead to more robust performance. Besides, though a certain spinning latency is inevitable in RoSense, it is lower than that of CPIX. Moreover, RoSense is universal for various applications and can work effectively under diverse settings as long as the LOS signal exists.

VII. Conclusion

In this article, we propose a brand-new universal method RoSense to refine the LOS signal phase for robust RFID sensing, by spinning the reader antenna. RoSense can work effectively under different settings, without any extra RF devices or offline training. Experimental results demonstrate that RoSense can achieve a remarkable performance gain for two typical sensing applications and outperform the state-of-the-art works.

Appendix
Changing Tendency of P_M and ψ Regarding α in (7)

First, we denote $A_i = \sqrt{p^2+q^2}\eta_i$ and (7) can be reformulated as

$$\begin{aligned}
&\sum_{i=1}^{N} 2\sqrt{p^2+q^2}\eta_i \cos(\beta_i-\alpha)\cos(2\pi ft-\delta_i)\\
&=\sum_{i=1}^{N} 2A_i\cos(\beta_i-\alpha)\cos(\delta_i)\cos(2\pi ft)\\
&\quad+\sum_{i=1}^{N} 2A_i\cos(\beta_i-\alpha)\sin(\delta_i)\sin(2\pi ft)\\
&=A\cos\left(2\pi ft-\arctan\frac{\sum_{i=1}^{N}2A_i\cos(\beta_i-\alpha)\sin(\delta_i)}{\sum_{i=1}^{N}2A_i\cos(\beta_i-\alpha)\cos(\delta_i)}\right).
\end{aligned}\tag{17}$$

Thus, the amplitude of $S_M(t)$ is

$$A=\sqrt{\left(\sum_{i=1}^{N}2A_i\cos(\beta_i-\alpha)\cos(\delta_i)\right)^2+\left(\sum_{i=1}^{N}2A_i\cos(\beta_i-\alpha)\sin(\delta_i)\right)^2}$$

and the phase shift of $S_M(t)$ is

$$\psi=\arctan\frac{\sum_{i=1}^{N}2A_i\cos(\beta_i-\alpha)\sin(\delta_i)}{\sum_{i=1}^{N}2A_i\cos(\beta_i-\alpha)\cos(\delta_i)}.$$

According to our definition of δ_i in Section III-A, we know that $\delta_i-\alpha$ is independent of α and $\delta_i+\alpha$ contains the component of 2α. So we define two constants $B_i=\beta_i-\alpha+\delta_i$ and $Z_i=(\delta_i-\beta_i+\alpha)-2\alpha$ which are independent of α. Then, we can transform A^2 into the following expressions:

$$\begin{aligned}
A^2&=\left(\sum_{i=1}^{N}A_i\cos(B_i)+\sum_{i=1}^{N}A_i\cos(Z_i+2\alpha)\right)^2\\
&\quad+\left(\sum_{i=1}^{N}A_i\sin(B_i)+\sum_{i=1}^{N}A_i\sin(Z_i+2\alpha)\right)^2\\
&=\left(\sum_{i=1}^{N}A_i\cos(B_i)+\sum_{i=1}^{N}A_i\cos(Z_i)\cos(2\alpha)\right.\\
&\qquad\left.-\sum_{i=1}^{N}A_i\sin(Z_i)\sin(2\alpha)\right)^2\\
&\quad+\left(\sum_{i=1}^{N}A_i\sin(B_i)+\sum_{i=1}^{N}A_i\sin(Z_i)\cos(2\alpha)\right.\\
&\qquad\left.+\sum_{i=1}^{N}A_i\cos(Z_i)\sin(2\alpha)\right)^2\\
&=\left(\tilde{A}\cos(2\alpha+H_1)+\sum_{i=1}^{N}A_i\cos(B_i)\right)^2\\
&\quad+\left(\tilde{A}\sin(2\alpha+H_1)+\sum_{i=1}^{N}A_i\sin(B_i)\right)^2\\
&=\left(\sum_{i=1}^{N}A_i\cos(B_i)\right)^2+\left(\sum_{i=1}^{N}A_i\sin(B_i)\right)^2+\tilde{A}^2\\
&\quad+\left(2\tilde{A}\sum_{i=1}^{N}A_i\right)\cos(2\alpha+H_1-H_2)
\end{aligned}\tag{18}$$

where

$$\tilde{A} = \sqrt{\left(\sum_{i=1}^{N} A_i \cos(Z_i)\right)^2 + \left(\sum_{i=1}^{N} A_i \sin(Z_i)\right)^2},$$

$$H_1 = \arctan \frac{\sum_{i=1}^{N} A_i \sin(Z_i)}{\sum_{i=1}^{N} A_i \cos(Z_i)}, \text{ and}$$

$$H_2 = \arctan \frac{\sum_{i=1}^{N} A_i \sin(B_i)}{\sum_{i=1}^{N} A_i \cos(B_i)}.$$

$\tilde{A}$, H_1, and H_2 are independent of α. Hence, the changing tendency of A^2 is determined by $\cos(2\alpha + H_1 - H_2)$. Based on the relationship between RSS and signal amplitude, the value of P_M is proportional to A^2. Accordingly, P_M changes nonlinearly and nonmonotonically with α.

Similarly, we can transform ψ as follows:

$$\begin{aligned}\psi &= \arctan \frac{\sum_{i=1}^{N} A_i \sin(B_i) + \sum_{i=1}^{N} A_i \sin(Z_i + 2\alpha)}{\sum_{i=1}^{N} A_i \cos(B_i) + \sum_{i=1}^{N} A_i \cos(Z_i + 2\alpha)} \\ &= \arctan \frac{\tilde{A} \sin(2\alpha + H_1) + \sum_{i=1}^{N} A_i \sin(B_i)}{\tilde{A} \cos(2\alpha + H_1) + \sum_{i=1}^{N} A_i \cos(B_i)}. \end{aligned} \tag{19}$$

Based on the monotonicity of the arc-tangent function, we only need to study the changing tendency of $Y = [\tilde{A} \sin(2\alpha + H_1) + \sum_{i=1}^{N} A_i \sin(B_i)]/[\tilde{A} \cos(2\alpha + H_1) + \sum_{i=1}^{N} A_i \cos(B_i)]$ regarding α. Denote $\hat{A} = \sqrt{(\sum_{i=1}^{N} A_i \cos(B_i))^2 + (\sum_{i=1}^{N} A_i \sin(B_i))^2}$ and we can obtain its derivative

$$\frac{\partial Y}{\partial \alpha} = \frac{2\tilde{A}^2 + 2\tilde{A}\hat{A} \cos(2\alpha + H_1 - H_2)}{\left(\tilde{A} \cos(2\alpha + \arctan H_1) + \sum_{i=1}^{N} A_i \cos(B_i)\right)^2}. \tag{20}$$

Therefore, it is uncertain whether the changing tendency of ψ is monotonic or not. If $\hat{A} \leq \tilde{A}$, ψ will monotonically increase with α. Otherwise, ψ will change nonmonotonically. Even so, the tendency must be nonlinear in terms of (19).

In addition, we can find that the changing tendencies of P_M and ψ in one period are evidently inconsistent through the above analysis.

REFERENCES

[1] T. Liu, Y. Liu, L. Yang, Y. Guo, and C. Wang, "BackPos: High accuracy backscatter positioning system," *IEEE Trans. Mobile Comput.*, vol. 15, no. 3, pp. 586–598, Mar. 2016.

[2] L. Yang, Y. Chen, X.-Y. Li, C. Xiao, M. Li, and Y. Liu, "Tagoram: Real-time tracking of mobile RFID tags to high precision using COTS devices," in *Proc. ACM Conf. Mobile Comput. Netw. (MobiCom)*, 2014, pp. 237–248.

[3] B. Xie *et al.*, "Tagtag: Material sensing with commodity RFID," in *Proc. ACM Conf. Embedded Netw. Sens. Syst. (SenSys)*, 2019, pp. 338–350.

[4] L. Shangguan, Z. Yang, A. X. Liu, Z. Zhou, and Y. Liu, "Relative localization of RFID tags using spatial-temporal phase profiling," in *Proc. USENIX Symp. Netw. Syst. Des. Implement. (NSDI)*, 2015, pp. 251–263.

[5] L. Shangguan and K. Jamieson, "The design and implementation of a mobile RFID tag sorting robot," in *Proc. ACM Conf. Mobile Syst. Appl. Serv. (MobiSys)*, 2016, pp. 31–42.

[6] C. Duan, L. Yang, Q. Lin, Y. Liu, and L. Xie, "Robust spinning sensing with dual-RFID-tags in noisy settings," *IEEE Trans. Mobile Comput.*, vol. 18, no. 11, pp. 2647–2659, Nov. 2019.

[7] L. Yang, Y. Li, Q. Lin, H. Jia, X.-Y. Li, and Y. Liu, "Tagbeat: Sensing mechanical vibration period with COTS RFID systems," *IEEE/ACM Trans. Netw.*, vol. 25, no. 6, pp. 3823–3835, Dec. 2017.

[8] S. Pradhan and L. Qiu, "RTSense: Passive RFID based temperature sensing," in *Proc. ACM Conf. Embedded Netw. Sens. Syst. (SenSys)*, 2020, pp. 42–55.

[9] J. Wang, L. Chang, S. Aggarwal, O. Abari, and S. Keshav, "Soil moisture sensing with commodity RFID systems," in *Proc. ACM Conf. Mobile Syst. Appl. Serv. (MobiSys)*, 2020, pp. 273–285.

[10] J. Wang, L. Chang, O. Abari, and S. Keshav, "Are RFID sensing systems ready for the real world?" in *Proc. ACM Conf. Mobile Syst. Appl. Serv. (MobiSys)*, 2019, pp. 366–377.

[11] A. Lazaro, D. Girbau, and D. Salinas, "Radio link budgets for UHF RFID on multipath environments," *IEEE Trans. Antennas Propag.*, vol. 57, no. 4, pp. 1241–1251, Apr. 2009.

[12] Z. Wang, M. Xu, N. Ye, R. Wang, and H. Huang, "RF-focus: Computer vision-assisted region-of-interest RFID tag recognition and localization in multipath-prevalent environments," *Proc. ACM Interact. Mobile Wearable Ubiquitous Technol.*, vol. 3, no. 1, pp. 1–30, 2019.

[13] J. Wang and D. Katabi, "Dude, where's my card? RFID positioning that works with multipath and non-line of sight," in *Proc. Annu. Conf. ACM Spec. Interest Group Data Commun. (SIGCOMM)*, 2013, pp. 51–62.

[14] Z. Luo, Q. Zhang, Y. Ma, M. Singh, and F. Adib, "3D backscatter localization for fine-grained robotics," in *Proc. USENIX Symp. Netw. Syst. Des. Implement. (NSDI)*, 2019, pp. 765–782.

[15] X. Fan, F. Wang, F. Wang, W. Gong, and J. Liu, "When RFID meets deep learning: Exploring cognitive intelligence for activity identification," *IEEE Wireless Commun.*, vol. 26, no. 3, pp. 19–25, Jun. 2019.

[16] H. Xu, D. Wang, R. Zhao, and Q. Zhang, "FaHo: Deep learning enhanced holographic localization for RFID tags," in *Proc. ACM Conf. Embedded Netw. Sens. Syst. (SenSys)*, 2019, pp. 351–363.

[17] G. Wang *et al.*, "A universal method to combat multipaths for RFID sensing," in *Proc. IEEE Int. Conf. Comput. Commun. (INFOCOM)*, 2020, pp. 277–286.

[18] EPC Global, "Specification for RFID air interface EPC^{TM} radio-frequency identity protocols class-1 generation-2 UHF RFID protocol for communications at 860 MHz–960 MHz," GS1, Brussels, Belgium, Rep., 2008.

[19] L. Ni, Y. Liu, Y. C. Lau, and A. Patil, "LANDMARC: Indoor location sensing using active RFID," in *Proc. IEEE Int. Conf. Pervasive Comput. Commun. (PerCom)*, 2003, pp. 407–415.

[20] S. Yang, M. Jin, Y. He, and Y. Liu, "RF-prism: Versatile RFID-based sensing through phase disentangling," in *Proc. IEEE Int. Conf. Distrib. Comput. Syst. (ICDCS)*, 2021, pp. 1053–1063.

[21] "Speedway revolution reader application note: Low level user data support," Application Notes, ImpinJ, Seattle, WA, USA, 2010.

[22] "ImpinJ Inc." [Online]. Available: http://www.impinj.com (Accessed: Feb. 16, 2022).

[23] "Alien Technology." [Online]. Available: http://www.alientechnology.com (Accessed: Feb. 16, 2022).

[24] D. M. Dobkin, *The RF in RFID: UHF RFID in Practice*. Amsterdam, The Netherlands: Newnes, 2012.

[25] C. Jiang, Y. He, S. Yang, J. Guo, and Y. Liu, "3D-OmniTrack: 3D tracking with COTS RFID systems," in *Proc. ACM/IEEE Int. Conf. Inf. Process. Sens. Netw. (IPSN)*, 2019, pp. 25–36.

[26] K. Cui, Y. Wang, Y. Zheng, and J. Han, "ShakeReader: 'Read' UHF RFID using smartphone," in *Proc. IEEE Int. Conf. Comput. Commun. (INFOCOM)*, 2021, pp. 1–10.

[27] L. Yang *et al.*, "Revisting tag collision problem in RFID systems," in *Proc. ACM Int. Conf. Parallel Process. (ICPP)*, 2010, pp. 178–187.

[28] C. Wang, L. Xie, K. Zhang, W. Wang, Y. Bu, and S. Lu, "Spin-antenna: 3D motion tracking for tag array labeled objects via spinning antenna," in *Proc. IEEE Int. Conf. Comput. Commun. (INFOCOM)*, 2019, pp. 1–9.

[29] "Laird Technologies." [Online]. Available: http://www.lairdtech.com/ (Accessed: Feb. 16, 2022).

[30] *Low Level Reader Protocol (LLRP)*, EPCglobal, Brussels, Belgium, 2010.

[31] L. Yang, P. Peng, F. Dang, C. Wang, X.-Y. Li, and Y. Liu, "Anti-counterfeiting via federated RFID tags' fingerprints and geometric relationships," in *Proc. IEEE Int. Conf. Comput. Commun. (INFOCOM)*, 2015, pp. 1966–1974.

[32] "ImpinJ Support." [Online]. Available: http://support.impinj.com/hc/en-us/articles/360000046899-Reader-Modes-Made-Easy (Accessed: Feb. 16, 2022).

[33] C. Duan, J. Liu, X. Ding, Z. Li, and Y. Liu, "Full-dimension relative positioning for RFID-enabled self-checkout services," *Proc. ACM Interact. Mobile Wearable Ubiquitous Technol.*, vol. 5, no. 1, pp. 1–23, 2021.

[34] B. Xie, J. Xiong, X. Chen, and D. Fang, "Exploring commodity RFID for contactless sub-millimeter vibration sensing," in *Proc. ACM Conf. Embedded Netw. Sens. Syst. (SenSys)*, 2020, pp. 15–27.
[35] U. Ha, J. Leng, A. Khaddaj, and F. Adib, "Food and liquid sensing in practical environments using RFIDs," in *Proc. USENIX Symp. Netw. Syst. Des. Implement. (NSDI)*, 2020, pp. 1083–1100.
[36] J. Liu, M. Chen, S. Chen, Q. Pan, and L. Chen, "Tag-compass: Determining the spatial direction of an object with small dimensions," in *Proc. IEEE Int. Conf. Comput. Commun. (INFOCOM)*, 2017, pp. 1–9.
[37] T. Wei and X. Zhang, "Gyro in the air: Tracking 3D orientation of batteryless Internet-of-Things," in *Proc. ACM Conf. Mobile Comput. Netw. (MobiCom)*, 2016, pp. 55–68.
[38] X. Chen, J. Liu, F. Xiao, S. Chen, and L. Chen, "Thermotag: Item-level temperature sensing with a passive RFID tag," in *Proc. ACM Conf. Mobile Syst. Appl. Serv. (MobiSys)*, 2021, pp. 163–174.
[39] W. Sun and K. Srinivasan, "Healthy diapering with passive RFIDs for diaper wetness sensing and urine pH identification," in *Proc. ACM Conf. Mobile Syst. Appl. Serv. (MobiSys)*, 2021, pp. 188–201.
[40] J. Guo, T. Wang, Y. He, M. Jin, C. Jiang, and Y. Liu, "TwinLeak: RFID-based liquid leakage detection in industrial environments," in *Proc. IEEE Int. Conf. Comput. Commun. (INFOCOM)*, 2019, pp. 883–891.
[41] X. Chen, J. Liu, X. Wang, H. Liu, D. Jiang, and L. Chen, "Eingerprint: Robust energy-related fingerprinting for passive RFID tags," in *Proc. USENIX Symp. Netw. Syst. Des. Implement. (NSDI)*, 2020, pp. 1101–1113.
[42] S. Pradhan, S. Li, and L. Qiu, "Rotation sensing using passive RFID tags," in *Proc. ACM Int. Symp. Theory Algorithmic Found. Protocol Des. Mobile Netw. Mobile Comput. (MobiHoc)*, 2021, pp. 71–80.

Yinan Zhu (Student Member, IEEE) received the B.E. degree from Zhejiang University of Technology, Hangzhou, China, in 2019, and the M.E. degree from Tsinghua University, Beijing, China, in 2022.

His research interests include RFID security, wireless sensing, and mobile computing.

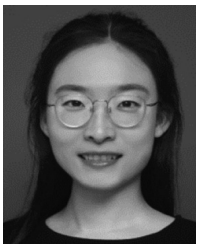

Chunhui Duan (Member, IEEE) received the B.S. and Ph.D. degrees from the School of Software, Tsinghua University, Beijing, China, in 2013 and 2018, respectively.

She was a Postdoctoral Research Fellow with Tsinghua University. She is currently an Associate Professor with the School of Computer Science and Technology, Beijing Institute of Technology, Beijing. Her research interests include RFID, Internet of Things, wireless sensing, and mobile computing.

Xuan Ding (Member, IEEE) received the bachelor's degree from the School of Software, Tsinghua University, Beijing, China, in 2008, and the Ph.D. degree from the Department of Computer Science and Technology, Tsinghua University in 2014.

He is currently a Research Assistant Professor with the School of Software, Tsinghua University. His research interests span privacy-aware computing, secure multiparty computation, blockchain, and RFID.

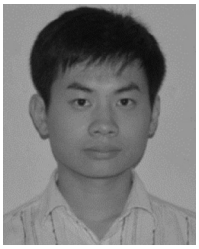

Zheng Yang (Fellow, IEEE) received the B.E. degree in computer science from Tsinghua University, Beijing, China, in 2006, and the Ph.D. degree in computer science from Hong Kong University of Science and Technology, Hong Kong, in 2010.

He is an Associate Professor with Tsinghua University. His main research interests include Internet of Things and mobile computing.

Dr. Yang is the PI of National Natural Science Fund for Excellent Young Scientist and has been awarded the State Natural Science Award (second class).